OPEN ACCESS

UNIVERSITY OF THE WEST of SCOTLAND
UWS

UWS Academic Portal

Enhancing the removal of Sb (III) from water

Zhang, Jun; Deng, Renjian; Ren, Bozhi; Yaseen, Mohammed; Hursthouse, Andrew

Published in:
Processes

DOI:
10.3390/pr8010044

Published: 01/01/2020

Document Version
Publisher's PDF, also known as Version of record

Link to publication on the UWS Academic Portal

Citation for published version (APA):
Zhang, J., Deng, R., Ren, B., Yaseen, M., & Hursthouse, A. (2020). Enhancing the removal of Sb (III) from water: a Fe3O4@HCO composite adsorbent caged in sodium alginate microbeads. *Processes*, *8*(1), [44]. https://doi.org/10.3390/pr8010044

General rights
Copyright and moral rights for the publications made accessible in the UWS Academic Portal are retained by the authors and/or other copyright owners and it is a condition of accessing publications that users recognise and abide by the legal requirements associated with these rights.

Take down policy
If you believe that this document breaches copyright please contact pure@uws.ac.uk providing details, and we will remove access to the work immediately and investigate your claim.

Download date: 02 Mar 2020

processes

MDPI

Article

Enhancing the Removal of Sb (III) from Water: A Fe_3O_4@HCO Composite Adsorbent Caged in Sodium Alginate Microbeads

Jun Zhang [1], Renjian Deng [1,2,*], Bozhi Ren [1], Mohammed Yaseen [3] and Andrew Hursthouse [1,3,*]

1 School of Civil Engineering, Hunan University of Science and Technology, Xiangtan 411201, China; z931021j@163.com (J.Z.); bozhiren@126.com (B.R.)
2 Hunan Jing Yi Environmental Protection High Tech Development Co. Ltd., Xiangtan,411201, China
3 School of Computing, Engineering & Physical Sciences, University of the West of Scotland, Paisley PA1 2BE, UK; mohammed.yaseen@uws.ac.uk
* Correspondence: 800912deng@sina.com (R.D.); andrew.hursthouse@uws.ac.uk (A.H.)

Received: 11 December 2019; Accepted: 26 December 2019; Published: 1 January 2020

Abstract: To remove antimony (Sb) ions from water, a novel composite adsorbent was fabricated from ferriferous oxide and waste sludge from a chemical polishing process (Fe_3O_4@HCO) and encapsulated in sodium alginate (SAB). The SAB adsorbent performed well with 80%–96% removal of Sb (III) ions within a concentration range of 5–60 mg/L. The adsorption mechanism of Sb (III) was revealed to be the synergy of chemisorption (ion exchange) and physisorption (diffusion reaction). The adsorption isotherms and kinetics conformed to the Langmuir isotherm and the pesudo-second-order kinetic model. Both initial pH and temperature influenced the adsorption performance with no collapse of microbeads within solution pH range 3–7. Most importantly for practical applications, these microspheres can be separated and recovered from aqueous solution by a magnetic separation technology to facilitate large-scale treatment of antimony-containing wastewater.

Keywords: ferriferous oxide polishing sludge; sodium alginate; microbeads; adsorption; antimony-containing wastewater

1. Introduction

Antimony (Sb) is a well-known, naturally occurring and highly toxic and carcinogenic metalloid element [1]. It occurs predominantly in two forms of oxidation states (+III and +V) in natural water bodies [2]. Long-term excessive intake of Sb can seriously affect human health, causing liver and lung injury and weakening of the human immune system [3]; thus, antimony is listed as a dangerous substance in many countries or by international organizations. Within the global context, China has significant reserves of antimony ores and ranks first in the world for the production of antimony. Long term high-intensity mining and smelting activities have produced a serious legacy of antimony pollution for China [4]. Hence, the prevention and purification of antimony-contaminated water is an issue requiring urgent attention. In addition, other sources of antimony pollution occur more frequently, at lower levels around industrial manufacturing of metallic and plastic components.

Purification of antimony-containing water has been extensively researched through a number of unit processes [5–8]. Among these technologies, adsorption is considered to be promising due to its simple operation, cost effectiveness and potentially eco-friendly applications [9]. Consequently many adsorbents, such as, activated carbon [10], metal oxides [11], natural minerals [12] and municipal sewage sludge [3] has been investigated for its removal from aqueous solution. As a frequently used adsorbent, incorporation of ferriferous oxide (Fe_3O_4) in water treatment combines good adsorption properties with the potential for magnetic separation from the liquid phase allowing re-use after

desorption of contaminants [13,14]. The ability for magnetic separation is a much more powerful approach to solid recovery than normal separation methods for instance sedimentation, filtration, etc. However, a number of studies have shown that Fe_3O_4 has limitations, since its sorption capability is comparatively low compared to emerging solid phases [15–19]. Therefore, research to identify improved adsorption capacity of Fe_3O_4 is a major opportunity [12].

Synthesis and preparation of iron-containing bimetal oxides can greatly improve adsorbent performance because of increasing the size of specific surface area and the number of hydroxyl groups, and creating a tunable surface charge [13,20,21]. It has also been shown that cerium-doped magnetic Fe_3O_4 adsorbents show promising adsorption capacity [20–24], and potential as an fine adsorbent specifically for Sb ions' removal [20,24]. Nevertheless, cerium is a less-common metal and its application is limited. Sludge from the waste water discharges from polishing stages in optical and electronics manufacture is a major source of release. It is estimated that China generates over 5.0×10^4 tons each year of sludge which is particularly rich in condensed cerium (Ce), mostly as hydrous ceric oxide (HCO: $CeO_2 \cdot nH_2O$, also known as cerium hydroxide).

In previous studies, we have successfully prepared Fe_3O_4@HCO adsorbent with good removal effect on Sb (III) [25], but Fe_3O_4@HCO adsorbent has some limitations, such as poor precipitation effect, easy hardening and weak regeneration ability. In order to solve the limitations of the application of Fe_3O_4@HCO adsorbent, we used sodium alginate (SA) microspheres prepared by the ion exchange method. SA is an anionic polymer, rich in algae-derived polysaccharide composed of beta-1, 4-D-mannuronic acid and α-1, 4-L guluronic acid, and the ratio of these two acids determine its characteristic properties for interacting with cations. Thus, SA readily complexes with cations such as divalent calcium, magnesium and zinc, with the potential to form gels for applications such as absorption and use in controlled drug release [26,27]. This latter application is further optimized because of SA having biocompatibility, biodegradability and non-toxicity properties [28]. Du used sodium alginate as carrier to immobilize sludge-based biomass carbon to prepare a new type of environmental friendly and economical adsorbent for copper removal, sodium alginate immobilized sludge carbon (SASC) [29]. Zhang applied sodium alginate to solidify activated carbon and bacteria and applied it to the treatment of waste-water containing Pb^{2+} [24]. Zhu used sodium alginate to immobilize Fe-Cu bimetal to overcome the shortcomings of low utilization rate, easy hardening and blockage of Fe0-pemeable reactive barrier (PRB), and studied the mechanism of Cr (VI) removal [30]. Lakouraj studied the adsorption of heavy metal ions by sodium alginate nano-gels and super paramagnetic nano-composites [31].

In this study, Fe_3O_4@HCO/SA modified microspheres (SAB) were prepared using the Fe_3O_4@HCO adsorbent and SA. We studied the physicochemical properties of the adsorbents, and the performance for Sb (III) removal from water solution was evaluated. This included sorption kinetics and capacity, mechanism of interaction, effects of the composition of the water matrix and the material stability. Collectively, it provides the scientific underpinning for the application of Fe_3O_4@HCO composites in the treatment of Sb dominated water pollution.

2. Materials and Methods

2.1. Preparation of Fe_3O_4@HCO Composite Adsorbent-Sodium Alginate Microbeads

A known amount of Fe_3O_4@HCO adsorbent and SA were weighed and ground in a mortar; then, mixed well in a beaker with water. The Fe_3O_4@HCO/SA composite liquid was obtained; the bubbles in the solution disappeared completely on leaving the solution to rest. SAB were prepared by the drop wise addition of the aqueous Fe_3O_4@HCO adsorbent-sodium alginate colloidal solution into a beaker containing calcium chloride solution (5%, *w/v*) using stirring. The microspheres were agitated in $CaCl_2$ solution for approximately 4 h until they were cross-linked completely. They were then collected and washed three or four times with distilled water and absolute ethanol. Lastly, they were dried at 50 °C.

The optimum concentration ratio of SA to Fe_3O_4@HCO adsorbent was determined by observing the morphology of microspheres dropped into calcium chloride solution and dried.

2.2. Characterization Methods

Particle morphology and crystallinity of SAB were characterized on a scanning electron microscope (SEM, Gemini SEM 500, Carl Zeiss AG, Oberkochen, Germany). Elements content on the surface of SAB were quantitatively measured using an energy dispersive spectrometer (EDS) spectrum analyzer (EDXA, Bruker XFlash 5010, Bruker AXS Microanalysis, Berlin, Germany). X-ray diffraction (XRD; D8 Advance, Brook AXS Ltd., Karlsruhe, Germany) was used to analyze the compounds present in the precipitate before and after adsorption of Sb (III) by SAB. The structures of surface functional groups and pore of SAB were determined by Fourier transform infrared spectroscopy (Nicolet 6700, Thermo Fisher, Waltham, Massachusetts, USA). X-ray photo-electron spectroscopy (XPS, Thermo Scietific: Esala 250Xi, Thermo Fisher, Waltham, Massachusetts, USA) spectra were used to investigate the surface elemental compositions and functional groups.

2.3. Batch Adsorption Experiments

An adsorption test was executed in a sequence batch device. The effects of pH (2–9), temperature (25 °C) and coexisting anions (NO^{3-}, $SO_4{}^{2-}$, $PO_4{}^{3-}$, $SiO_3{}^{2-}$) on Sb (III) removal performance onto SAB were investigated. The 1.0 g/L antimony standard reserve solution was prepared by dissolving $C_8H_4K_2O_{12}Sb_2$ (2.738 g) in 1.0 L distilled water. The solutions of different concentrations were obtained by appropriate dilution, and the pH was adjusted using either 0.1 mol L^{-1} hydrochloric acid or 0.1 mol L^{-1} sodium hydroxide solution. The interfering ions used in the experiment were all anionic sodium salts. All experiments were repeated in three groups.

Sorption isotherm experiments were carried out by adding 0.4 g of SAB adsorbent into 100 mL of Sb (III) solution (pH 7.0 ± 0.1) and varied from 5 to 100 mg/L. It was then oscillated for 144 h at 150 revolutions per minute at 25 °C; the residual Sb concentration in water was measured as mentioned before. Kinetic experiments were performed by adding 0.4 g of SAB adsorbent into 100 mL of 100 mg/L Sb (III) solution (pH 7.0 ± 0.1). Samples were taken at the following intervals: 3, 6, 9, 12, 24, 36, 48, 72, 96, 120 and 144 h, after start of the reaction and then filtered to measure the residual Sb (III) concentration in solution. The removal rate (R%) and adsorption at equilibrium (q_e) of Sb (III) can be obtained by the following formula:

$$R(\%) = \frac{C_0 - C_e}{C_0} \times 100 \quad (1)$$

$$q_e = \frac{V(C_0 - C_e)}{m}, \quad (2)$$

where C_0 and C_e (mg/L) are the initial and equilibrium concentrations of Sb (III) in the aqueous, respectively; q_e (mg/g) is the amount of adsorptions capacity; V (L) is the volume of the solution; m (g) is the dry-weight of the adsorbent.

2.4. Analysis

In accordance with the literature, the concentration of antimony was measured by an atomic fluorescence photometer, with which the minimum detection concentration was less than 1 μg/L [32]. All samples were analyzed within one day after sampling, and blank control experiments were performed with distilled water. The recovery of Sb (III) was over 90.0% using this test.

3. Results and Discussion

3.1. SAB Spheroidizing Effect

The spheroidization of Fe_3O_4@HCO and SA microspheres with different concentrations is shown in Table 1 and Figure A1. It can be seen from Table 1 that SAB microspheres have a better spheroidizing effect when the concentration of the Fe_3O_4@HCO to SA ratio is between 1.25 and 1.33 (Figure A1). Considering the shape of the pellets, the concentration of Fe_3O_4@HCO was 2.5%, and that of SA was 2%.

Table 1. Spheroidization of Fe_3O_4@HCO and SA microspheres with different concentrations.

SA (%)	Fe_3O_4@HCO (%)			
	1.5	**2**	**2.5**	**3**
1.5	Slightly tailed	Better results	Better results	Slightly tailed
2	Better results	Better results	Better results	General effect
2.5	Tailing phenomenon	Tailing phenomenon	Tailing phenomenon	Tailing phenomenon

3.2. Characterization

SEM images of SAB before and after Sb (III) adsorption are shown in Figure 1. Before adsorption, SAB was mainly granular with a smooth surface (Figure 1a). Also, as shown in Figure 1a, some cross-linking is visible and porosity is high, which indicates that Fe_3O_4@HCO adsorbent was encapsulated in sodium alginate network [15]. At the same time, the X-ray analysis (EDS) (Figure 1a) showed that the main elements of SAB were O (38.86%), Ce (13.07%), Fe (13.46%), C (8.82%) and Cl (9.21%), implying that the chemical compositions of this adsorbent iron oxides and cesium oxides. The surface morphology of SAB adsorbed Sb (III) changed to some extent, and the surface was rough and the porosity was reduced (Figure 1b). EDS spectra show that the weight percentage of Sb increases to 2.46%, which indicates that Sb is adsorbed by SAB [33].

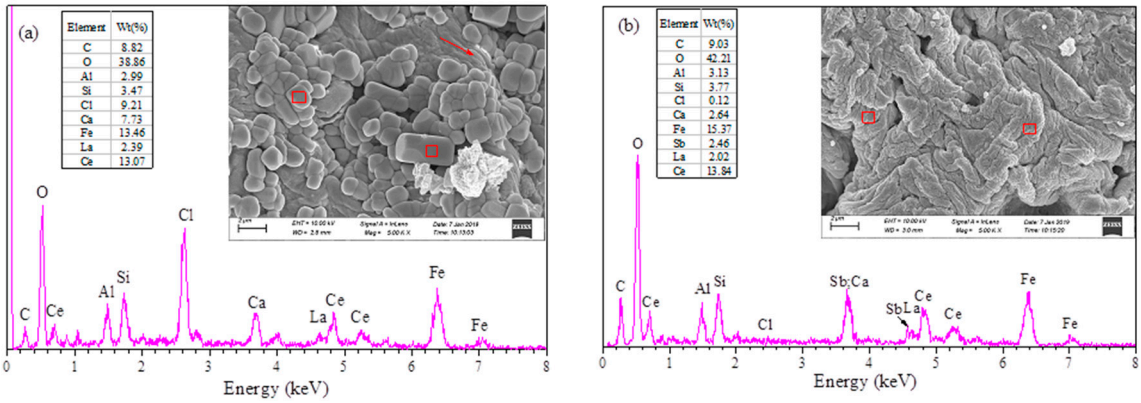

Figure 1. SEM-EDS images of SAB before (**a**) and after (**b**) Sb (III) adsorption.

The XRD patterns before and after the adsorption of Sb (III) by SAB are shown in Figure 2a. For SAB, five diffraction peaks were observed across 2θ (20°–60°) of 26.57°, 28.50°, 33.07°, 47.44° and 56.33°, which agreed with the characteristic peaks of Fe_3O_4 and CeO_2 [15]. Moreover, the XRD spectra of SAB were retrieved and analyzed by Jade (Materials Data Inc., Livermore, CA, American), and it was found that CeO_2, Fe_3O_4 and $FeCeO_4$ were present within SAB. Therefore, it can be inferred that $FeCe_2O_4$ was synthesized by the compound reaction of CeO_2 and Fe_3O_4 in the process of SAB synthesis. Phase analysis of the product residues showed that $CeSbO_3$, SbO_3, $FeSbO_4$ and $FeSbO_6$ were in the remaining material. It can be inferred that CeO_2, Fe_3O_4 and $FeCeO_4$ can react with Sb (III)

in the process of SAB adsorbing Sb (III). In conclusion, the adsorption of Sb (III) by SAB is mainly because of the synergistic adsorption of Fe oxides and Ce oxides in SAB.

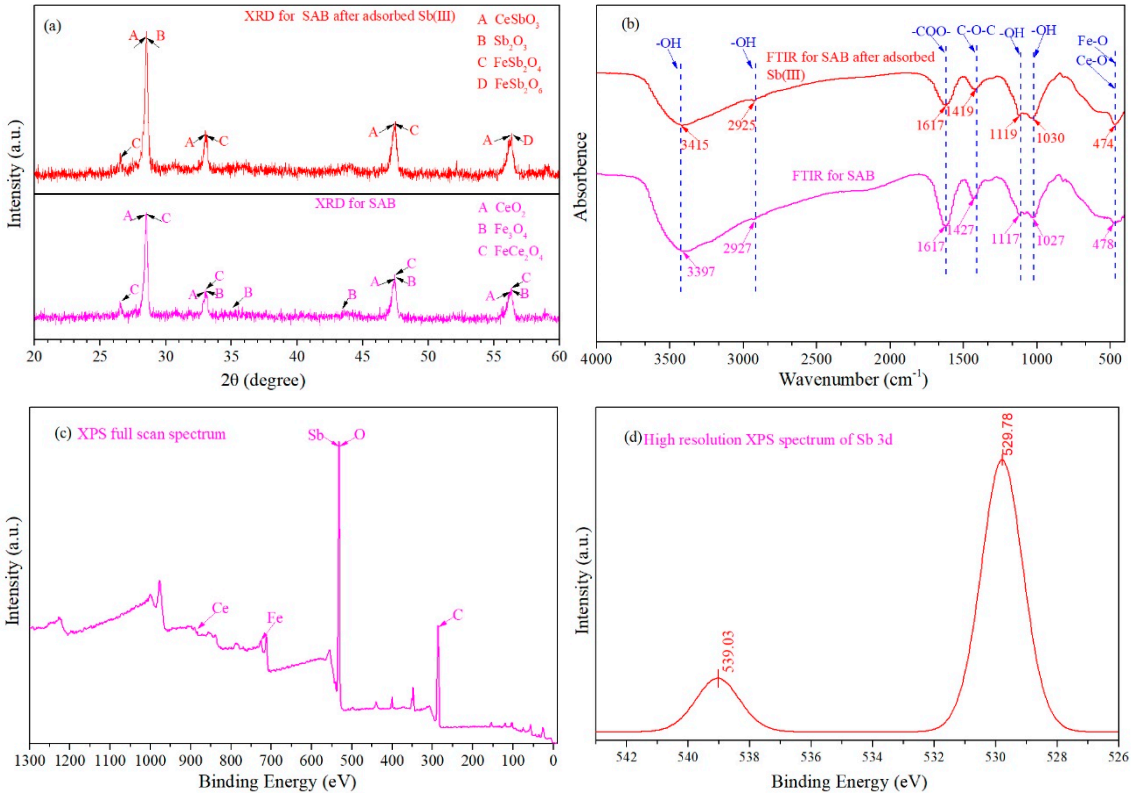

Figure 2. (**a**) XRD patterns, (**b**) FTIR spectra and (**c**) XPS full scan spectrum and (**d**) high resolution XPS spectrum of Sb 3d.

The Figure 2b shows the FTIR spectra before and after the adsorption of Sb (III) by SAB Figure 2b. As shown in Figure 2b, the absorption peaks which appear at 3397 cm^{-1} and 2927 cm^{-1} can be attributed to the stretching vibration of hydroxyl groups in free water [34]. The absorption peaks at 1617 cm^{-1}, 1427 cm^{-1} and 1117 cm^{-1} are the bending and vibration absorption peaks of –COO–, C–O–C and –OH in SA, respectively [35]. The absorption peak at 1027 cm^{-1} is the bending and vibration absorption peak of –OH corresponding to iron [34]. The absorption peak at 478 cm^{-1} is the bending and vibration absorption peak of Fe-O offset in the presence of Ce, which may be caused by the increase of cation vacancy in the lattice [36], indicating that Ce occupies the original position of Fe and forms new bonds with the surrounding atom [20]. Meanwhile, the C–O–C absorption peak at 1427 cm^{-1}, after SAB adsorbed Sb (III) shifted slightly as shown the Figure 3b. It can be inferred that Sb (III) complexation occurs with functional groups in SAB.

XPS, as we know, can measure the composition of the residual products after SAB has adsorbed Sb (III) [15,20]. As shown in Figure 2c, full scan spectra show that Ce, Fe, Sb, O and C are present in the remaining products, indicating that Sb is adsorbed by SAB. To learn more about the electronic states of the Sb (III) element, high resolution spectral analysis of Sb was also carried out (Figure 2d). The binding energies of Sb ($3d_{5/2}$) and Sb ($3d_{3/2}$) detected by XPS were 529.78 and 539.03 eV, respectively. According to the chemical state database of XPS, the residual product has Sb (V) on the surface, and the original water solution used in the experiment was Sb (III) solution. This indicates that there was redox reaction in the process of adsorption, which is basically consistent with the results of Qi [20].

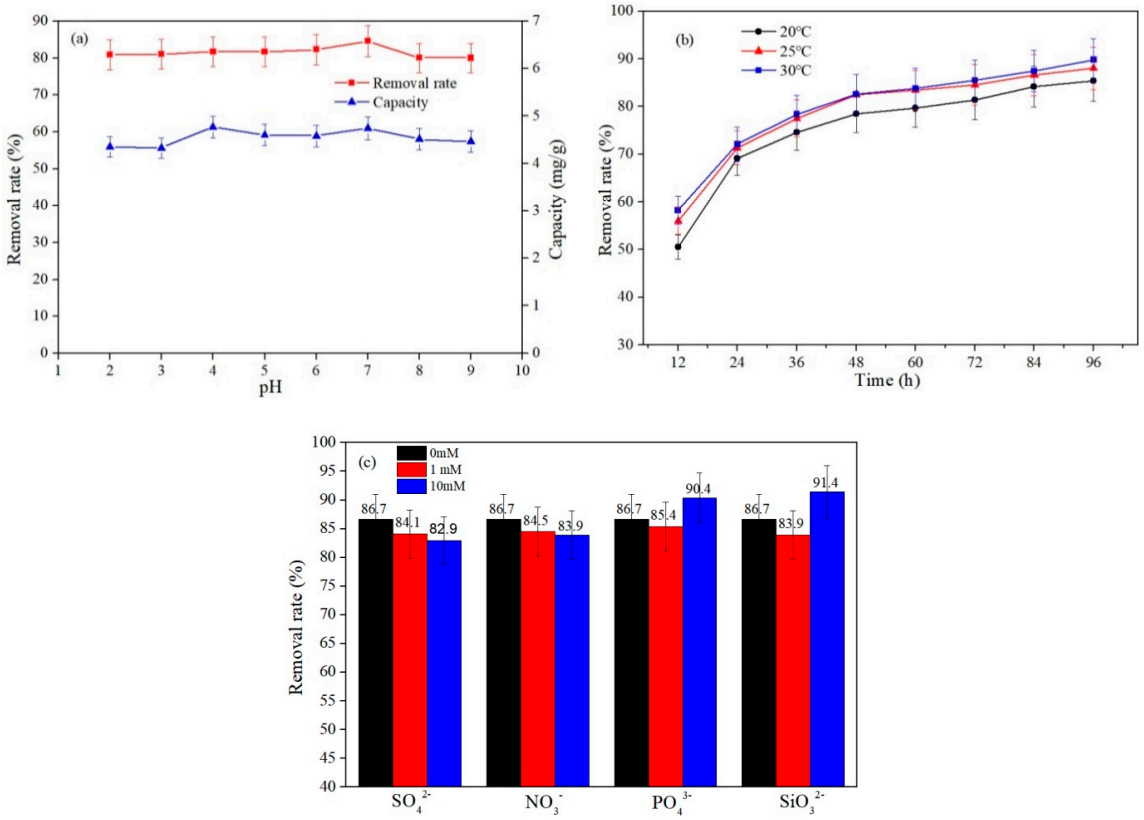

Figure 3. The effects of pH (**a**), temperature (**b**) and coexisting ions (**c**) on the adsorption properties of Sb (III) ions by SAB.

3.3. The Effects of pH, Temperature and Coexisting Ions

Initial pH is one of the most important parameters affecting adsorption performance and adsorption capacity. For the study, experiments were performed at pH values varying from 3 to 9. As seen in Figure 3a, the adsorption ability of SAB microspheres is most effective within the pH range of 4– 7, but decreases when pH is greater than 7 or less than 3. The SAB microspheres have the strongest adsorption capacity for Sb (III) ions at pH of 7, consistent with Deng's previous research [21]. Sb (III) mainly exists in the form of $Sb(OH)_2^+$ when pH is 2 [37], thereby competing with H^+ and $Sb(OH)_2^+$; hence, reducing the Sb (III) removal efficiency [38]. At pH of more than 9, the oxidation of Sb (III) was reinforced [39], and thus it inhibited the production of iron oxyhydroxide and reduced the solubility of iron ions, thereby causing in a decrease of Sb (III)'s adsorbing performance [21] by Fe_3O_4@HCO. So, SAB adsorption of Sb (III) can be applied to a wide range pH values and presents a broad potential application range.

The effect of temperature on the Sb (III) removal rate is readily seen in Figure 3b. The removal efficiencies at 20 °C and 30 °C are 85.4% and 89.8%, respectively. The results show that with ascending temperature, the removal rate of Sb (III) increases, indicating that the adsorption of Sb (III) is an endothermic process in this adsorption system, consistent with previous study of the adsorption of metal ions by an iron matrix [33].

Considering the existence of ions in antimony-containing wastewater, we investigated the effect of some coexisting ions (NO^{3-}, SO_4^{2-}, PO_4^{3-}, SiO_3^{2-}) on the adsorption of Sb (III) by SAB, as indicated in Figure 3c. The results show that the added anions, including NO^{3-} and SO_4^{2-}, have no significant effect on Sb (III) sequestration. This could be because that the interaction between NO^{3-} and SO_4^{2-} with SAB is mainly through outer complexation, and thus, the effect on the adsorption of Sb (III) is not significant [6,40]. Together, 1 mM PO_4^{3-} and 1 mM SiO_3^{2-} inhibited the adsorption of Sb (III) by SAB, but again, the effect was not great. This may be because low the concentrations of PO_4^{3-} and SiO_3^{2-}

can compete with Sb (III) for the sites of SAB through specific adsorption. In contrast, 10 mM PO_4^{3-} and 10 mM SiO_3^{2-} resulted in a small enhancement on the adsorption of Sb (III) by SAB. For PO_4^{3-}, this may be because the higher concentration of Na_3PO_4 solution can dissolve SAB microspheres [41], resulting in the increase of contact area between SAB and Sb (III), promoting the adsorption of Sb (III) to a certain extent. However the promotion mechanism of SiO_3^{2-} on the adsorption of Sb (III) by SAB remains to be further studied.

3.4. Adsorption Isotherms

Isothermal adsorption models can provide information on adsorption mechanisms, surface properties and affinities of adsorbents [21,23,33]. In this research, the adsorption of Sb (III) solutions at different concentration was studied at pH 7, at 25 °C, over 144 h. To determine the mechanistic parameters related to Sb (III) adsorption, we used Langmuir model, Freundlich model and D-R model to study the relationship between Sb (III) adsorption in an aqueous solution and its residual amount in the adsorption process [15]. The equilibrium constants and correlation coefficients of adsorption isotherm model of SAB for Sb (III) are shown in Figure 4 and Table 2. The experimental results show that the adsorption data is a linear fit, and thus agrees well with Langmuir adsorption isotherm model ($R^2 > 0.99$), indicating that the adsorption process of Sb (III) by SAB belongs to a single layer adsorption process, which is consistent with the conclusions of other researchers [20,21,33,42]. Additionally, the Q_{max} value for SAB was found to be 17.338 mg g^{-1}, which was close to the experimental value (15.368 mg g^{-1}), which demonstrated that it has good adsorption properties in comparison with other containing or iron loaded composite adsorbents, such as $MnFe_2O_4$ adsorption Sb (III) (10.66 mg g^{-1}) [43] and nano FeOOH modified zeolite adsorption Sb (III) (7.17 mg g^{-1}) [19]. The Freundlich adsorption isotherm model shows that Sb (III) is easily adsorbed by SAB ($1/n < 0.5$), which provides a good condition for adsorption [44]. The data of D-R adsorption isotherm model further indicated that the adsorption process belongs to chemical adsorption (E > 16 KJ/mol) [45].

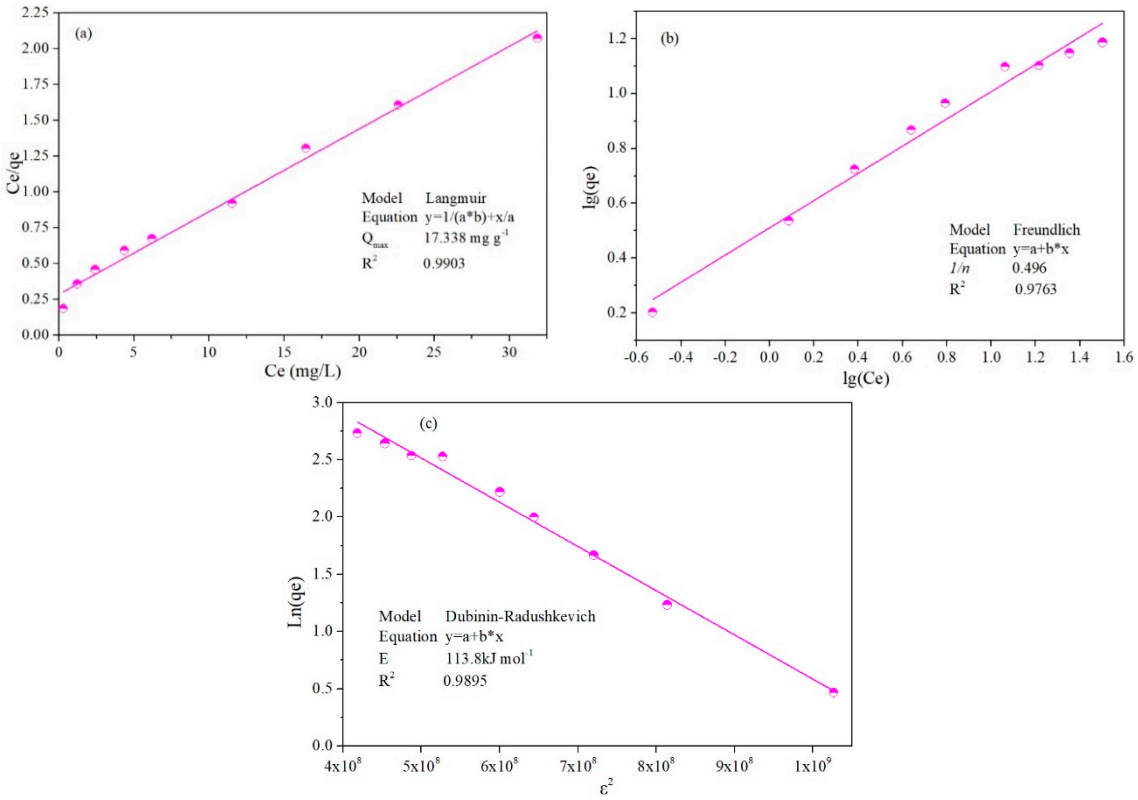

Figure 4. Adsorption isotherms for Sb (III) by SAB adsorbent: (**a**) Langmuir isotherms, (**b**) Freundlish isotherms, (**c**) D-R isotherms.

Table 2. Isotherms parameters for adsorption of Sb (III) onto SAB.

Models Typle	Langmuir	Freundlich	D-R
Parameter values	Q_{max} = 17.338 mg g^{-1} b = 0.201 L mg^{-1} R^2 = 0.9903	K_f = 3.24 1/n = 0.496 R^2 = 0.9763	$\beta = -3.86\times10^{-9}$ mol^2 kJ^{-2} Q_S = 85.09 mg g^{-1} E = 113.8 KJ mol^{-1} R^2 = 0.9895

3.5. Adsorption Process and Kinetics

Adsorption kinetic models can be utilized to fit experimental data, and thus provide potential rate profile, and information on the adsorption mechanism and the feasibility of chemical adsorption in the process of adsorption [46]. In order to understand the process, in this study the kinetics were analyzed using pseudo-first-order kinetics, pseudo-second-order kinetics, Elovich kinetics and intra-particle diffusion kinetics [15]. The kinetic models of Sb (III) absorption on SAB are shown in Figure 5, with the equilibrium constants and correlation coefficients of the kinetic models described in Table 3. The results show that the pseudo-second-order kinetics and Elovich kinetics fit better with the experimental data ($R^2 > 0.99$), which indicates that the parameters were better relatively. It also shows that the adsorption process could be approximated the pseudo-second-order and Elovich kinetics [33,47]. It was surmised that the soak up on SAB for Sb (III) was predominantly chemical. At the same time, the kinetic constants and parameters of intra-particle diffusion in Figure 5 and Table 3 indicate that the internal diffusion dominates but is not the only adsorption mechanism in the process of SAB adsorption for Sb (III). Initial rapid reaction phase is usually interpreted as a high-affinity site adsorption or a precise adsorption of the adsorbent on the adsorbent surface [20], and the surface adsorption process is affected by the thickness of the boundary layer. Furthermore, the rate of SAB adsorption for Sb (III) is controlled by the boundary layer effect and external mass transfer effect [38].

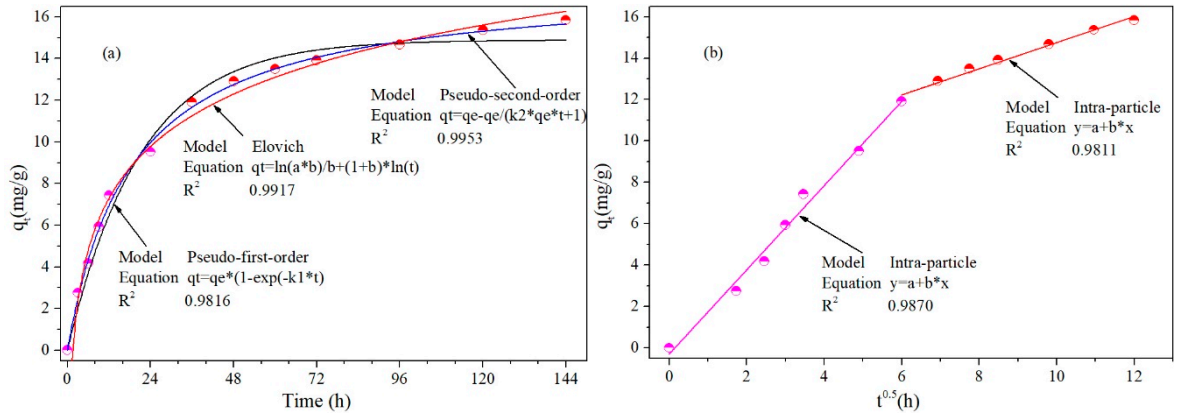

Figure 5. Adsorption kinetics of Sb (III) on SAB adsorbent: (**a**) pseudo-first-order kinetics, pseudo-second-order kinetics and Elovich kinetics, (**b**) intra-particle diffusion kinetics.

Table 3. Calculated kinetic parameters for the adsorption of Sb (III) onto SAB.

Models	Pseudo-First-Order	Pseudo-Second-Order	Elovich	Intra-Particle Diffusion
Parameters	q_e = 14.886 mg g^{-1} K_1 = 0.048 min^{-1} R^2 = 0.982	q_e = 17.661 mg g^{-1} K_2 = 0.003 min^{-1} R^2 = 0.995	a = 2.266 b = 0.277 R^2 = 0.992	a_1 = −0.299 mg g^{-1} K_{41} = 2.035 mg g^{-1} $h^{-0.5}$ R^2 = 0.987 a_2 = 8.427 mg g^{-1} K_{42} = 0.632 mg g^{-1} $h^{-0.5}$ R^2 = 0.981

3.6. Adsorption Mechanisms

Compared with the results of different isothermal adsorption models, the experimental data for Sb (III) sorption onto SAB are consistent with the Langmuir adsorption isothermal model, and fit best with pseudo-second-order model. It can be shown that the whole adsorption process of Sb (III) is a single layer adsorption process controlled by the chemical reaction at the solid-liquid interface [20,48]. Meanwhile, the Elovich model also fits well, indicating that there is diffusion reaction in the adsorption process [20,49].

The FTIR results of SAB have shown that there are many surface hydroxyl groups on its surface, and abundant surface hydroxyl groups (alginate) are the main reason for its superior adsorption performance for antimony [50]. The XRD results showed that the residual products after adsorption contained $FeSb_2O_4$, $FeSb_2O_6$ and $CeSbO_3$. It can be speculated that in the adsorption process, there is an ion exchange reaction between $Sb(OH)_3^0$ and the surface hydroxyl group of Fe_3O_4 [8,51]. In addition, HCO in SAB also exchanges anionic ligands with SbO_3^{3-} [20,52].

4. Conclusions

In brief, Fe_3O_4@HCO adsorbent was synthesized by an improved co-precipitation method and encapsulated into sodium alginate microbead (SAB), with the aim of removing antimony ions from an aqueous solution. The SAB adsorbent was found to have a high removal rate (80%–96%) for Sb (III) solution within the concentration range 5–60 mg L^{-1}. The adsorption process of SAB fits perfectly with the Langmuir and pseudo-second-order kinetics models. The removal principle for Sb (III) was synergy of chemisorption (ion exchange) and physisorption (diffusion reaction). The synthetic process for the preparation of SAB is simple; costs are low; and it is eco-friendly, as the main components, Fe_3O_4 and polishing sludge, are content affluent and environmentally friendly. In addition, the loaded sorbent can be easily recovered from water.

Author Contributions: Conceived and designed the study, R.D. and J.Z.; Analyzed the data, B.R. and M.Y.; Wrote the paper, R.D. and J.Z.; Assessed data and reviewed the manuscript, A.H. All authors have read and agreed to the published version of the manuscript.

Funding: This study was financially supported by the National Natural Science Foundation of China (No. 41672350), the scientific research project of the Hunan Provincial Education Department (No. 18A184) and the Chinese Postdoctoral Science Foundation (No. 2018M632961).

Conflicts of Interest: The authors declare no conflict of interest.

Appendix A

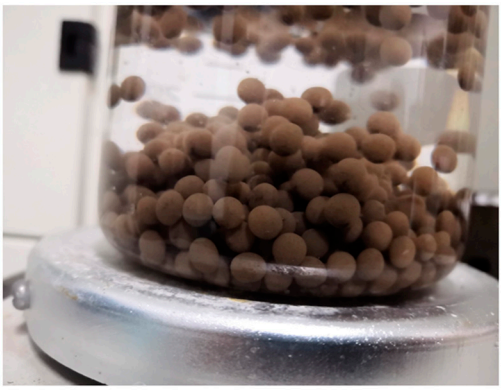

Figure A1. SAB balling effect.

References

1. Hu, X.Y.; Kong, L.H.; He, M.C. Kinetics and Mechanism of Photopromoted Oxidative Dissolution of Antimony Trioxide. *Environ. Sci. Technol.* **2014**, *48*, 14266–14272. [CrossRef] [PubMed]
2. Filella, M.; Belzile, N.; Chen, Y. Antimony in the environment: A review focused on natural waters: I. Occurrence. *Earth Sci. Rev.* **2002**, *57*, 125–176. [CrossRef]
3. Ungureanu, G.; Santos, S.; Boaventura, R.; Botelho, C. Arsenic and antimony in water and wastewater: Overview of removal techniques with special reference to latest advances in adsorption. *J. Environ. Manag.* **2015**, *151*, 326–342. [CrossRef] [PubMed]
4. Wu, Z.J.; He, M.C.; Guo, X.J.; Zhou, R.J. Removal of antimony (III) and antimony (V) from drinking water by ferric chloride coagulation: Competing ion effect and the mechanism analysis. *Sep. Purif. Technol.* **2010**, *76*, 184–190. [CrossRef]
5. Mendil, D.; Bardak, H.; Tuzen, M.; Soylak, M. Selective speciation of inorganic antimony on tetraethylenepentamine bonded silica gel column and its determination by graphite furnace atomic absorption spectrometry. *Talanta* **2013**, *107*, 162–166. [CrossRef] [PubMed]
6. Miao, Y.; Han, F.; Pan, B.; Niu, Y.; Nie, G. Antimony(V) removal from water by hydrated ferric oxides supported by calcite sand and polymeric anion exchanger. *J. Environ. Sci.* **2014**, *26*, 307–314. [CrossRef]
7. Du, X.; Qu, F.S.; Liang, H.; Li, K.; Yu, H.R.; Bai, L.M.; Li, G.B. Removal of antimony (III) from polluted surface water using a hybrid coagulation-flocculation-ultrafiltration (CF-UF) process. *Chem. Eng. J.* **2014**, *254*, 293–301. [CrossRef]
8. Guo, X.J.; Wu, Z.J.; He, M.C.; Meng, X.G.; Jin, X.; Zhang, J. Adsorption of antimony onto iron oxyhydroxides: Adsorption behavior and surface structure. *J. Hazard. Mater.* **2014**, *276*, 339–345. [CrossRef]
9. Herath, I.; Vithanage, M.; Bundschuh, J. Antimony as a global dilemma: Geochemistry, mobility, fate and transport. *Environ. Pollut.* **2017**, *223*, 545–559. [CrossRef]
10. Navarro, P.; Alguacil, F.J. Adsorption of antimony and arsenic from a copper electrorefining solution onto activated carbon. *Hydrometallurgy* **2002**, *66*, 101–105. [CrossRef]
11. Fan, H.T.; Sun, Y.; Tang, Q.; Li, W.L.; Sun, T. Selective adsorption of antimony (III) from aqueous solution by ion-imprinted organic–inorganic hybrid sorbent: Kinetics, isotherms and thermodynamics. *J. Taiwan. Inst. Chem. Eng.* **2014**, *45*, 2640–2648. [CrossRef]
12. Leyva, A.G.; Marrero, J.; Smichowski, P.; Cicerone, D. Sorption of Antimony onto Hydroxyapatite. *Environ. Sci. Technol.* **2001**, *35*, 3669–3675. [CrossRef] [PubMed]
13. Mehta, D.; Mazumdar, S.; Singh, S.K. Magnetic adsorbents for the treatment of water/wastewater-A review. *J. Water Process Eng.* **2015**, *7*, 244–265. [CrossRef]
14. Kharissova, O.V.; Dias, R.; Kharisov, B.I. Magnetic adsorbents based on micro- and nano-structured materials. *RSC Adv.* **2014**, *5*, 6695–6719. [CrossRef]
15. Yang, H.J.; Li, H.Y.; Zhai, J.L.; Sun, L.; Zhao, Y.; Yu, H.W. Magnetic prussian blue/graphene oxide nanocomposites caged in calcium alginate microbeads for elimination of cesium ions from water and soil. *Chem. Eng. J.* **2014**, *246*, 10–19. [CrossRef]
16. Wan, C.L.; Wang, L.; Lee, D.J. Fungi aerobic granules and use of Fe (III)-treated granules for biosorption of antimony(V). *J. Taiwan Inst. Chem. Eng.* **2014**, *45*, 2610–2614. [CrossRef]
17. You, D.; Min, X.Y.; Liu, L.L.; Ren, Z. New insight on the adsorption capacity of metallogels for antimonite and antimonate removal: From experimental to theoretical study. *J. Hazard. Mater.* **2018**, *346*, 218. [CrossRef]
18. Han, L.F.; Sun, H.R.; Ro, K.S.; Libra, J.A.; Xing, B.S. Removal of antimony (III) and cadmium (II) from aqueous solution using animal manure-derived hydrochars and pyrochars. *Bioresour. Technol.* **2017**, *234*, 77–85. [CrossRef]
19. Chmielewská, E.; Tylus, W.; Drábik, M. Structure investigation of nano-FeO(OH) modified clinoptilolite tuff for antimony removal. *Microporous Mesoporous Mater.* **2017**, *248*, 222–233. [CrossRef]
20. Qi, Z.L.; Joshi, T.P.; Liu, R.P.; Liu, H.J.; Qu, J.H. Synthesis of Ce (III)-doped Fe_3O_4 magnetic particles for efficient removal of antimony from aqueous solution. *J. Hazard. Mater.* **2017**, *329*, 193–204. [CrossRef]
21. Deng, R.J.; Jin, C.S.; Ren, B.Z.; Hou, B.L. The Potential for the Treatment of Antimony-Containing Wastewater by Iron-Based Adsorbents. *Water* **2017**, *9*, 794. [CrossRef]
22. Zhang, Y.; Yang, M.; Dou, X.X.; He, H.; Wang, D.S. Arsenate adsorption on an Fe-Ce bimetal oxide adsorbent: Role of surface properties. *Environ. Sci. Technol.* **2005**, *39*, 7246–7253. [CrossRef] [PubMed]

23. Chen, B.; Zhu, Z.L.; Guo, Y.W.; Qiu, Y.L.; Zhao, J.F. Facile synthesis of mesoporous Ce-Fe bimetal oxide and its enhanced adsorption of arsenate from aqueous solutions. *J. Colloid Interface Sci.* **2013**, *398*, 142–151. [CrossRef] [PubMed]
24. Zhang, Y.; Dou, X.M.; Zhao, B.; Yang, M.; Takayama, T.; Kato, S. Removal of arsenic by a granular Fe-Ce oxide adsorbent: Fabrication conditions and performance. *Chem. Eng. J.* **2010**, *162*, 164–170. [CrossRef]
25. Zhang, J.; Deng, R.J.; Ren, B.Z.; Hou, B.L.; Andrew, H. Preparation of a novel Fe_3O_4/HCO composite adsorbent and the mechanism for the removal of antimony (III) from aqueous solution. *Sci. Rep.* **2019**, *9*, 1–11. [CrossRef]
26. Chan, L.W.; Jin, Y.; Heng, P.W.S. Cross-linking mechanisms of calcium and zinc in production of alginate microspheres. *Int. J. Pharm.* **2002**, *242*, 255–258. [CrossRef]
27. Sun, W.; Xing, J.; Zou, H.H.; Chen, L.C. Study on Sodium Alginate Gel Bead Removing Cr (VI). *Mod. Agric. Sci. Technol.* **2015**, *208*, 215.
28. İnal, M.; Erduran, N. Removal of various anionic dyes using sodium alginate/poly (N-vinyl-2-pyrrolidone) blend hydrogel beads. *Polym. Bull.* **2015**, *72*, 1–18. [CrossRef]
29. Du, S.W.; Zhou, H.; Peng, Y.Q.; Xiong, C.Q.; Wei, D.N.; Huang, H.L. Adsorption property of sodium aliginate immobilized sludge carbon with copper. *Environ. Eng.* **2017**, *35*, 37–42.
30. Zhu, W.H.; Wang, X.R.; Dong, L.F.; Wang, Q.; He, F. Mechanism of copper-iron bimetallic particles immobilized by sodium alginate in removal of Cr (VI). *China Environ. Sci.* **2013**, *33*, 1965–1971.
31. Lakouraj, M.M.; Mojerlou, F.; Zare, E.N. Nanogel and superparamagnetic nanocomposite based on sodium alginate for sorption of heavy metal ions. *Carbohydr. Polym.* **2014**, *106*, 34–41. [CrossRef] [PubMed]
32. Xi, J.H.; He, M.C.; Lin, C.Y. Adsorption of antimony (III) and antimony(V) on bentonite: Kinetics, thermodynamics and anion competition. *Microchem. J.* **2011**, *97*, 85–91. [CrossRef]
33. Deng, R.J.; Shao, R.; Ren, B.Z.; Andrew, H. Adsorption of Antimony (III) onto Fe (III)-Treated Humus Sludge Adsorbent: Behaviorand Mechanism Insights. *Pol. J. Environ. Stud.* **2019**, *28*, 577–586. [CrossRef]
34. Hu, X.X. Study on the performance and mechanism of the removal of antimony from mine waste water by a new type of Fe-Cu binary oxide. Master's Thesis, Hunan University of Science and Technology, Xiangtan, China, June 2016.
35. Wang, Q.; Zhu, S.Z.; Yang, W.J.; Zhou, Y.F. The Removal of Cr (VI) from Aqueous Solution by Magnetic Ferroferric Oxide@ Sodium Alginate Composite Adsorbent. *J. China West Norm. Univ.* **2017**, *38*, 282–287.
36. Anushree; Kumar, S.; Sharma, C. Synthesis, characterization and catalytic wet air oxidation property of mesoporous $Ce_{1-x}Fe_xO_2$ mixed oxides. *Mater. Chem. Phys.* **2015**, *155*, 223–231. [CrossRef]
37. Farquhar, M.L.; Charnock, J.M.; Livens, F.R.; Vaughan, D.J. Mechanisms of arsenic uptake from aqueous solution by interaction with goethite, lepidocrocite, mackinawite, and pyrite: An X-ray absorption spectroscopy study. *Environ. Sci. Technol.* **2002**, *36*, 1757. [CrossRef]
38. Fan, H.T.; Sun, W.; Jiang, B.; Wang, Q.J.; Li, D.W.; Huang, C.C. Adsorption of antimony (III) from aqueous solution by mercapto-functionalized silica-supported organic-inorganic hybrid sorbent: Mechanism insights. *Chem. Eng. J.* **2016**, *286*, 128–138. [CrossRef]
39. Leuz, A.K.; Mönch, H.; Johnson, C.A. Sorption of Sb (III) and Sb(V) to Goethite: Influence on Sb (III) Oxidation and Mobilization. *Environ. Sci. Technol.* **2006**, *40*, 7277–7282. [CrossRef]
40. Li, J.L.; Bao, H.L.; Xiong, X.M.; Sun, Y.K.; Guan, X.H. Effective Sb (V) immobilization from water by zero-valent iron with weak magnetic field. *Sep. Purif. Technol.* **2015**, *151*, 276–283. [CrossRef]
41. Tao, Y.F.; Yao, Y.; Ding, Y.F.; Liu, Q. Preparation of Ketorolac Tromethamine Alginate-chitosan Microcapsules. *Chin. J. Pharm.* **2006**, *37*, 401–403.
42. Li, Y.C.; Geng, B.; Hu, X.X. Preparation and characterization of iron-copper binary oxide and its effective removal of antimony (III) from aqueous solution. *Water Sci. Technol.* **2016**, *74*, 393–401. [CrossRef] [PubMed]
43. Rooygar, A.A.; Mallah, M.H.; Abolghasemi, H.; Safdari, J. New "Magmolecular" Process for the Separation of Antimony (III) from Aqueous Solution. *J. Chem. Eng. Data* **2014**, *59*, 3545–3554. [CrossRef]
44. Anirudhan, T.S.; Suchithra, P.S.; Radhakrishnan, P.G. Synthesis and characterization of humic acid immobilized-polymer/bentonite composites and their ability to adsorb basic dyes from aqueous solutions. *Appl. Clay Sci.* **2009**, *43*, 336–342. [CrossRef]
45. Shan, C.; Ma, Z.Y.; Tong, M.P. Efficient removal of trace antimony (III) through adsorption by hematite modified magnetic nanoparticles. *J. Hazard. Mater.* **2014**, *268*, 229–236. [CrossRef] [PubMed]

46. Vasiliu, S.; Bunia, I.; Racovita, S.; Neagu, V. Adsorption of cefotaxime sodium salt on polymer coated ion exchange resin microparticles: Kinetics, equilibrium and thermodynamic studies. *Carbohydr. Polym.* **2011**, *85*, 376–387. [CrossRef]
47. Zhao, Z.; Wang, X.; Zhao, C.; Zhu, X.; Du, S. Adsorption and desorption of antimony acetate on sodium montmorillonite. *J. Colloid Interface Sci.* **2010**, *345*, 154–159. [CrossRef] [PubMed]
48. Ho, Y.S. Second-order kinetic model for the sorption of cadmium onto tree fern: A comparison of linear and non-linear methods. *Water Res.* **2006**, *40*, 119–125. [CrossRef]
49. Xu, W.; Wang, H.J.; Liu, R.P.; Zhao, X.; Qu, J.H. The mechanism of antimony (III) removal and its reactions on the surfaces of Fe-Mn Binary Oxide. *J. Colloid Interface Sci.* **2011**, *363*, 320–326. [CrossRef]
50. Bée, A.; Talbot, D.; Abramson, S.; Dupuis, V. Magnetic alginate beads for Pb (II) ions removal from wastewater. *J. Colloid Interface Sci.* **2011**, *362*, 486–492. [CrossRef]
51. Mittal, V.K.; Bera, S.; Narasimhan, S.V.; Velmurugan, S. Adsorption behavior of antimony (III) oxyanions on magnetite surface in aqueous organic acid environment. *Appl. Surf. Sci.* **2013**, *266*, 272–279. [CrossRef]
52. Zhen, Q.; Ouyang, T.; Lin, J.D. Adsorption Characteristics of Arsenic in Water by Cerous Hydroxide. *Environ. Sanit. Eng.* **2008**, *16*, 13–15.

© 2020 by the authors. Licensee MDPI, Basel, Switzerland. This article is an open access article distributed under the terms and conditions of the Creative Commons Attribution (CC BY) license (http://creativecommons.org/licenses/by/4.0/).